

The low temperature elastic anomalies in solid helium

Eric Varoquaux*

CNRS and CEA-IRAMIS-DRECAM, Service de Physique de l'État Condensé,
Centre d'Études de Saclay, 91191 Gif-sur-Yvette Cedex (France)

(Dated: July 21, 2021)

The elastic properties of hcp ^4He samples have been shown to display various anomalies. As the temperature is lowered below ~ 0.2 K, the elastic shear modulus appears to stiffen and the moment of inertia appears to drop in a concomitant manner. The former phenomenon is taken as evidence for the pinning of dislocations, the latter, for the appearance of supersolidity. The close relationship between these two observables is studied within the framework of classical deformable-body mechanics. A model based on the formation by plastic flow of extremely soft quasi-planar, inter-connected layers of dislocations is solved analytically and numerically. This model relates quantitatively the change in moment of inertia to the drop in elastic constant and can account for most experimental observations. Other situations, in which its relevance may seem more doubtful, are discussed.

PACS numbers: 67.80-s, 61.72.Hh, 62.40.+i, 67.90.+z

I. INTRODUCTION

Helium makes an intriguing solid. Both ^4He and ^3He isotopes crystallise from the liquid at absolute zero under a pressure of 24.5 and 34.5 bars respectively. They form hexagonal close-packed (hcp) crystals with similar elastic properties. These crystals are very soft, owing to their small densities and weak atomic interactions. The paucity of slip directions causes crystals with the hcp structure to be quite brittle: they fracture very readily. This combination of softness and brittleness in the helium crystals make them very prone to plastic deformation and the formation of dislocation lines.

Because of the fast boson exchange in solid ^4He and the presence of defects, the possibility that a Bose-Einstein condensate would form within the crystalline lattice below a certain temperature was raised by a number of authors, starting with Penrose and Onsager in the fifties.¹ These authors argued that superfluid coherence, or off-diagonal long-range order (ODLRO), would not occur in an ideally perfect crystal but possibly could in a distorted lattice. Although the proof that they gave was criticised by others,²⁻⁴ it marked the beginning of a long-lasting search, both theoretical and experimental, for features that could reveal the existence of such a “supersolid” state in a suitably disordered crystal.

This search received strong renewed impetus after the observation by Kim and Chan (see the reviews [5]) of an anomaly in the rotational inertia of ^4He solid samples as seen as a period shift in high-quality-factor torsional oscillators (TO). The increase in the period of the oscillator resonance below a temperature of ~ 0.2 K, now observed by many groups, is taken to signal the decoupling of part of the helium mass from the motion of the oscillator bob. This effect, first discussed by Leggett⁴ and called in the present context non-classical rotational inertia (NCRI), occurs in a number of TO experiments with widely different sizes and geometries including very confined ones such as those of Vycor or sintered gold.

In the framework of the time-honoured two-fluid model for superfluidity,⁶ such an observation would signal the appearance of a superfluid-like fraction in the solid. Such a “condensate” would settle to rest and decouple from the oscillator walls as the temperature is lowered, reducing the moment of inertia. This interpretation is born out by the fact that, if the oscillator geometry is modified by a partition blocking the closed loop along which the superflow is supposed to take place,^{7,8} the effect disappears. Also, NCRI is not observed when the oscillator is filled with ^3He instead of ^4He ,^{7,9} which constitutes a strong hint that quantum statistics plays a fundamental role.

The TO measurements do seem to suggest that some form of superfluid behaviour occurs in solid ^4He below $0.1\sim 0.2$ K but other unambiguous manifestations of the existence of a true superfluid component, such as a non-dissipative DC-flow,¹⁰⁻¹³ or a persistent current, a second sound¹⁴ or fourth sound¹⁵ mode, the fountain effect, the signature of a BEC condensate on neutron¹⁶⁻¹⁸ or X-ray diffractograms¹⁹ are still lacking in spite of the efforts and ingenuity of many research groups.

Shear modulus measurements in solid helium at low temperature provide another class of anomalous elastic properties. These measurements span many years, starting with the early work of Wanner *et al.*²⁰ soon followed by others.²¹⁻²⁵ They have recently been extended to the same range of temperatures and ^3He impurity concentrations as the TO experiments.²⁶⁻²⁹ A marked decrease in the shear modulus G takes place in most samples of hcp ^4He upon warming from $T \sim 0$. The magnitude of the softening varies from sample to sample, depending in particular on the ^3He impurity content x_3 and the cooling history. The drop in G can be spectacular, down to less than 20 % from the $T \simeq 0$ value.^{21,25,28,29}

Day and Beamish²⁶ have argued that the T and x_3 dependence of G were mimicking closely those of the period shifts in TO experiments. In fact, the striking similarities between the shear modulus and the TO resonance

frequency drops make it hard not to believe that the two phenomena are somehow related. Direct experimental studies of this possible connection have led to diverging conclusions.^{30–33}

This article³⁴ outlines one possible such link between those two different mechanical properties of hcp ⁴He. It differs from similar attempts by other workers^{35–37} because it recognises from the start that the large drop in G requires the bunching of dislocation lines into extended quasi-planar highly deformable sheets, as described in Sec. (II). The consequences of these assumed defects are derived analytically for the shear modulus drop and for the apparent change of inertia in Sec. (III). These two quantities can thus be directly linked to one another. Numerical values are derived in Sec. (IV), where it is shown that this simple model may account quantitatively for a number of experimental observations. The model does not explain readily certain classes of experiments, notably those in confined geometries, and also the absence of inertia anomaly in solid ³He. Some speculations on these topics are offered in Sec. (V).

II. SOFT LAYER MODEL

II.1. Planar layers of dislocations

As mentioned above, the two helium crystals are very soft: the longitudinal and transverse sound velocities, in the 200 to 500 m/s range, are low. They are also very fragile: the yield strength is of the order of 0.2~0.5 bar,^{38,39} or very much less depending on the experimental conditions.⁴⁰ Dislocations appear readily under very weak mechanical perturbations or thermally induced stress. Plastic flow takes place during the formation and subsequent cooling of the solid helium sample. In the process, dislocations form and migrate.

Early sound propagation measurements in hcp ⁴He in the 5-50 MHz frequency range^{20,23,41,42} have revealed an anomalous temperature dependence below 1 K of the longitudinal sound velocity. This anomaly has been attributed to the unpinning of the dislocation lines as the trapped ³He impurities escape from the dislocation cores by thermal activation. This interpretation is well documented through the work of many authors^{22,24,25} and, more recently, by Syshchenko *et al.*⁴³.

The analysis of the high-frequency sound propagation measurements yields typical values²³ $\sim 10^6$ cm⁻² for the density of dislocation lines Λ and $5 \cdot 10^{-4}$ cm for the average distance between the nodes of the dislocation network L_N , assumed random and homogeneously distributed. The dimensionless quantity ΛL_N^2 is thus found of the order of ~ 0.25 .

Lower frequency measurements^{21,22,25} interpreted in the same manner with the help of the following relation for the change of the effective shear elastic constant G_{eff}

relative to the $T = 0$ value G ,⁴⁴

$$G/G_{\text{eff}} = 1 + 24(1 - \nu)\Omega\Lambda L_N^2/\pi^3, \quad (1)$$

give, assuming a value of 0.3 for the Poisson ratio ν and with the highest value for the orientation parameter $\Omega \leq 1/2$, much larger values of the quantity ΛL_N^2 . The shear modulus measurements by M.A. Paalanen, D.J. Bishop, and H.W. Dail²⁵ were carried out at a low frequency of 331 Hz and lead to a value of $\Lambda L_N^2 \gtrsim 1.0$ to 2.5 depending on samples. More recent measurements^{26,28,45,46} have confirmed these results. A softening of 86 % has been observed in an ultra-pure monocrystalline ⁴He sample by Rojas *et al.*²⁹ at frequencies in the 10-20 kHz range. In this extreme situation, the quantity ΛL_N^2 would exceed 20 using the same values for ν and Ω as above.

These values of ΛL_N^2 , obtained at long wavelengths, are much larger than the upper limit for a dense hexagonal network of dislocations, which espouses the underlying lattice symmetry. As shown in the Appendix, this limit is $1/\sqrt{2}$ for an ideal hcp network. The corresponding upper limit of G/G_{eff} as given by Eq.(1) is 1.2, which falls short of observations^{21,25,28,29} by a wide margin: edge dislocation lines escape from their preferential homogeneous hexagonal network structure and become quite extended.

This anomaly clearly points towards the formation of inhomogeneous dislocation structures. The dislocation lines collect in dense arrays, such as the mosaic structure that form along the boundaries between grains with slightly misaligned lattice vectors,⁴⁷ or, more generally, in extended planar structures. This rearrangement takes place during the formation of the hcp ⁴He samples and under thermal stress during cool-down.

It has been shown by numerical simulations of dislocation dynamics, notably by Amadeo and Ghoniem,^{48,49} that dislocations collect into different planar structures according to different applied perturbations. Planar arrays composed of sets of dislocation dipoles lying in planes containing the direction of the critical resolved shear stress form under monotonic stress conditions. Other types of structures, slip bands of parallel dislocation lines or dislocation cells, may appear under cyclic perturbations, provided, *e.g.*, by mechanical vibrations. These planar defects have been observed in a number of metallurgical samples.⁴⁷ Their phenomenology is well documented, as reviewed, *e.g.*, by Takeuchi and Argon⁵⁰ and others. Such dislocation substructures have also been observed in hcp ⁴He by X-ray topography by Iwasa *et al.*⁵¹ and by transmission Laue diffraction by Bossy *et al.*⁵².

These defect structures are thicker than the Franck networks that separate two grain boundaries of low-tilt angle. They are quite different from the random network assumed in the Granato-Lücke model,⁴⁴ as already mentioned. They can be viewed as resulting from the propagation of dislocation pileups under thermal stress in a way similar to the formation of cracks in usual hcp metals.⁵³ Solid helium exists only under positive pressure

and does not actually crack. Other types of extended defects appear and enable the crystal to yield in the deformation directions imposed by the rigid wall boundaries.

The dislocation arrays formed in such a manner are densely packed and have a high density of long dislocation lines; dislocations interact strongly and are organised in extended structures of parallel lines. They become extremely mobile when unadorned of the ^3He impurities that pin them to the lattice at $T \lesssim 0.2$ K and when unhampered by thermally excited phonons that prevail at $T \gtrsim 0.8$ K. Following the same line of reasoning that leads to Eq.(1), the resulting large values of ΛL_N^2 lead to very soft and easily deformable layers. These layers separate regions with depleted dislocation densities but of enhanced crystalline quality in which deformation also occurs quite readily,²⁹ at least in the directions of easy glide, but with the geometrical limit $\Lambda L_N^2 \lesssim 2^{-1/2}$.

II.2. Strain standing waves: homogeneous case

The simple model to be studied below assumes the existence of quasi-planar dislocation structures that facilitate both plastic and elastic deformations. To make the problem easily tractable analytically, a fully-planar geometry is assumed: the helium sample is taken to be confined between two parallel plane walls located at $z = 0$ and $z = R$ and extending to infinity along the x and y axes. The deformation u induced in the sample depends on z and t only (see Fig. 1); the problem is one-dimensional and easily solvable.

Shear stresses and strains are produced in the sample either by moving one plane, *e.g.*, that at $z = 0$ (which would be the transmitter in the shear modulus experiment) with respect to the $z = R$ plane, held steady (which would be the receiver). Torsional oscillator experiments are mimicked by moving both bounding walls in unison, letting the sample inertia develop internal stresses.

If the helium sample is homogeneous with a density ρ and a shear modulus G independent of position and time (no visco-elastic effect, no internal structure), the deformation $u(z, t)$ obeys the following partial differential equation:

$$\rho \frac{\partial^2 u}{\partial t^2} = G \frac{\partial^2 u}{\partial z^2}. \quad (2)$$

This equation describes the propagation of transverse plane waves with dispersion relation $\omega^2 = c_T^2 k^2$ and $c_T^2 = G/\rho$. The harmonic solution of Eq.(2) at frequency $\omega/2\pi$ is the sum of two counter-propagating waves:

$$u(z, t) = (u_{0+} e^{-ikz} + u_{0-} e^{ikz}) e^{i\omega t} = u(z) e^{i\omega t}. \quad (3)$$

The constants of integration for shear measurements u_{0+}^s and u_{0-}^s are then given by

$$\frac{u_{0+}^s}{e^{ikR}} = \frac{-u_{0-}^s}{e^{-ikR}} = \frac{u_0}{e^{ikR} - e^{-ikR}} = \bar{u}_0, \quad (4)$$

and the solution of Eq.(2) for the deformation as a function of z can then be expressed under the following form:

$$u(z) = u_0 \frac{\sin k(R-z)}{\sin kR}. \quad (5)$$

The stress in the solid is derived from the deformation, still disregarding the time dependence:

$$\sigma(z) = G \frac{du}{dz} = -k u_0 G \frac{\cos k(R-z)}{\sin kR}. \quad (6)$$

The force per unit area acting on the receiver is the opposite of that acting on the body, namely the internal stress:

$$F_R = -\sigma(R) = \frac{k u_0 G}{\sin kR}, \quad (7)$$

so that the measured effective shear elastic modulus G_{eff} is such that:

$$\frac{G}{G_{\text{eff}}} = \frac{u_0}{R} \frac{G}{F_R} = \frac{\sin kR}{kR} \simeq 1 - \frac{\rho \omega^2 R^2}{6G} + \dots \quad (8)$$

Equation (8) describes the change of the effective shear modulus at finite frequency due to the elastic response of the body. In the limit $\omega \rightarrow 0$, G_{eff} reduces to G . For $kR = \pi$, the body is set into resonance and, as damping has been neglected, the effective shear modulus diverges. Higher frequency modes are not considered here.

For torsional oscillator measurements this elastic response of the body becomes the dominant effect. In these experiments the two walls at $z = 0$ and $z = R$ are set into identical motion $u_0 e^{i\omega t}$. The solution to Eq.(2) that satisfies the boundary conditions

$$u(z)|_{z=0} = u(z)|_{z=R} = u_0 \quad (9)$$

can be written with the help of the following relations

$$\frac{u_{0+}^M}{1 - e^{ikR}} = \frac{-u_{0-}^M}{1 - e^{-ikR}} = \frac{u_0}{e^{ikR} - e^{-ikR}} = \bar{u}_0. \quad (10)$$

In particular, the stress $\sigma(z)$ is found to be:

$$\sigma(z) = G \frac{du}{dz} = -k G u_0 \frac{\cos k(R-z) - \cos kz}{\sin kR}. \quad (11)$$

The quantity actually measured in the TO type of experiments is the back-action of the sample on the measuring device, namely the total force $F_X + F_R$ exerted by the solid helium on both walls. This force is expressed, per unit area, by

$$F_X + F_R = \sigma(0) - \sigma(R) = 2k G u_0 \frac{1 - \cos kR}{\sin kR} \quad (12)$$

$$\simeq \rho R \omega^2 u_0 \left[1 + \frac{\rho \omega^2 R^2}{12G} + \dots \right]. \quad (13)$$

The meaning of Eqs.(12) and (13) is made clear by the prefactor of the right-hand side Eq.(13): $\omega^2 u_0$ is the acceleration amplitude, ρR the ‘‘bare’’ inertial mass M_I per

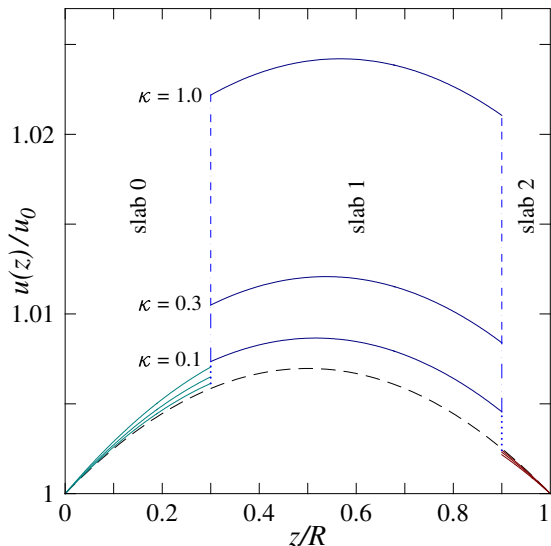


FIG. 1. Forms of the stationary wave in TO's experiments pictured as the relative displacement $u(z)/u_0$ for z varying from 0 to R for various dimensionless compliances κ of the soft layers, taken to be equal, for $R = 1$ cm at a frequency of one kHz ($kR = 0.2354$). The soft layers lay at $z_1 = 0.3R$ and $z_2 = 0.9R$, at the interfaces between slab 0, left, slab 1, middle, and slab 2, right. The dash-dot lines mark the discontinuities of $u(z)$. The dash-dash line represents the elastic behaviour with no soft layers.

unit area and, in the square bracket, the elastic correction at finite frequency. This “effective mass” correction increases with frequency up to the resonance at $kR = \pi$ where it becomes very large.

The shear modulus and effective mass corrections are related through Eqs.(8) and (12). Taking, *e.g.*, $R = 1$ cm, a frequency $\omega/2\pi = 1$ kHz, at a density $\rho = 0.194$ g/cm² for which $c_T = 267$ m/s, the effect of shear elasticity on the effective mass amounts to $4.6 \cdot 10^{-3}$, which is not insignificant. To a drop by 20% in G corresponds an apparent change in the mass by $\sim 10^{-3}$.

II.3. Soft layers

To account for the effect of highly deformable dislocation structures, the model is extended by introducing two soft layers at z_1 and z_2 parallel to the rigid cell walls, as depicted in Fig. 1. The slabs of solid helium that these soft layers delimit have the elastic properties of the homogeneous crystal discussed in subsection II.2 above.

Strain and stress are continuous functions at the interface between the slab of dislocation-free crystal and the soft layer. Denoting the shear modulus in the soft

layer G_s , shear plane waves propagate with wave vector $k_s = \sqrt{\rho/G_s}$. The propagation of the deformation-stress vector, $[u(z), \sigma(z)]$, in the layer of thickness d is described by the transfer matrix

$$\mathbf{M}(d) = \begin{bmatrix} \cos k_s d & (1/k_s G_s) \sin k_s d \\ -k_s G_s \sin k_s d & \cos k_s d \end{bmatrix}.$$

Although the problem of finding how plane waves propagate through the stack of slabs depicted in Fig. 1 is formally solved by multiplying transfer matrices such as $\mathbf{M}(d)$, it saves a number of algebraic steps to let the thickness d and the modulus G_s go to zero in such a way that d/G_s remains constant and equal to α . The effect of the soft layer is then lumped into a discontinuous jump in the deformation proportional to the local stress, described, for the layer at z_1 , by

$$\begin{aligned} u(z_1 + d) &= u(z_1) + \alpha_1 \sigma(z_1), \\ \sigma(z_1 + d) &= -k_s^2 d G_s u(z_1) + \sigma(z_1), \end{aligned} \quad (14)$$

In the limit $d \rightarrow 0$, the last equality expresses the continuity of stress across the infinitely thin layer while the displacement experiences a discontinuity. These boundary conditions, which could have been anticipated, also apply to the soft layer at z_2 with slip parameter α_2 . In the following, the soft layers will be described by their compliances α_i/R , which are such that the parameters $\kappa_i = \alpha_i G/R$ are dimensionless quantities.

III. MODEL ANALYSIS

III.1. Wave propagation through the sample

With the boundary conditions, Eqs.(14), describing the soft layers, the propagation of the propagating and counter-propagating waves through the three slabs of homogeneous crystal with shear modulus G and obeying no-slip boundary conditions at the walls can be found by straightforward algebra.

Wave propagation in slab 0, between $z = 0$ and z_1 as shown in Fig. 1, is represented by Eq.(3), which involves two integration constants u_{0+} and u_{0-} , the amplitudes of the counter-propagating plane waves with pulsation ω and wavevectors $\pm k$. Similar solutions obtain in slab 1 between z_1 and z_2 , and in slab 2 between z_2 and $z = R$, involving constants u_{1+} , u_{1-} , and u_{2+} , u_{2-} respectively.

The amplitudes of the propagating and counter-propagating waves in slab 2 are linearly related to those in slab 0:

$$\begin{aligned} u_{2+} &= \delta_{11} u_{0+} + \delta_{12} u_{0-}, \\ u_{2-} &= \delta_{21} u_{0+} + \delta_{22} u_{0-}. \end{aligned} \quad (15)$$

The deformation discontinuity at the soft layer at z_1 yields the following relations:

$$\begin{aligned} u_1(z_1) &= u_{1+}e^{-ikz_1} + u_{1-}e^{ikz_1} = u_{0+}(1 - i\kappa_1kR)e^{-ikz_1} + u_{0-}(1 + i\kappa_1kR)e^{ikz_1}, \\ \sigma(z_1) &= -ikG \left(u_{0+}e^{-ikz_1} - u_{0-}e^{ikz_1} \right) = -ikG \left(u_{1+}e^{-ikz_1} - u_{1-}e^{ikz_1} \right). \end{aligned}$$

Similar relations hold between u_{1+} , u_{1-} , and u_{2+} , u_{2-} . Eliminating u_{1+} and u_{1-} leads to the following expressions for the coefficients δ_{ij} of the matrix that describes wave propagation through the stack of slabs 0, 1, 2:

$$\delta_{11} = \left(1 - i\frac{\kappa_1}{2}kR\right) \left(1 - i\frac{\kappa_2}{2}kR\right) + \frac{\kappa_1\kappa_2}{4}k^2R^2 e^{2ik(z_2 - z_1)} = \delta'_{11} + i\delta''_{11}, \quad (16a)$$

$$\delta_{12} = i\frac{\kappa_1}{2}kR \left(1 - i\frac{\kappa_2}{2}kR\right) e^{2ikz_1} + i\frac{\kappa_2}{2}kR \left(1 + i\frac{\kappa_1}{2}kR\right) e^{2ikz_2} = \delta'_{12} + i\delta''_{12}, \quad (16b)$$

$$\delta_{21} = -i\frac{\kappa_1}{2}kR \left(1 + i\frac{\kappa_2}{2}kR\right) e^{-2ikz_1} - i\frac{\kappa_2}{2}kR \left(1 - i\frac{\kappa_1}{2}kR\right) e^{-2ikz_2} = \delta^*_{12}, \quad (16c)$$

$$\delta_{22} = \left(1 + i\frac{\kappa_1}{2}kR\right) \left(1 + i\frac{\kappa_2}{2}kR\right) + \frac{\kappa_1\kappa_2}{4}k^2R^2 e^{-2ik(z_2 - z_1)} = \delta^*_{11}, \quad (16d)$$

The matrix $\Delta = \|\delta_{ij}\|$, Eq.(16), describing wave propagation in a conservative time-reversal invariant system, is unitary and has determinant unity:

$$\delta_{11}\delta_{22} - \delta_{12}\delta_{21} = 1. \quad (17)$$

III.2. Shear modulus

For shear modulus measurements, the no-slip condition at the walls reads:

$$\begin{aligned} u_{0+} + u_{0-} &= u_0, \\ u_{2+}e^{-ikR} + u_{2-}e^{ikR} &= 0 \\ &= (\delta_{11}e^{-ikR} + \delta_{21}e^{ikR})u_{0+} + (\delta_{12}e^{-ikR} + \delta_{22}e^{ikR})u_{0-}, \end{aligned}$$

relations from which the integration constants u_{0+} and u_{0-} can be derived:

$$\begin{aligned} \frac{u_{0+}^S}{\delta_{12}e^{-ikR} + \delta_{22}e^{ikR}} &= \frac{-u_{0-}^S}{\delta_{11}e^{-ikR} + \delta_{21}e^{ikR}} \\ &= \frac{u_0}{(\delta_{12} - \delta_{11})e^{-ikR} - (\delta_{21} - \delta_{22})e^{ikR}} = \tilde{u}_0. \end{aligned} \quad (18)$$

The quantities u_{0+}^S and u_{0-}^S expressed by Eqs.(18) now include the effect of the soft layers and should not be confused with those given by Eq.(4), which do not. The shear stress at the receiver $\sigma(R)$ is given by

$$\sigma(R) = G \frac{du}{dz} \Big|_R = -ikG(u_{2+}e^{-ikR} - u_{2-}e^{ikR}).$$

Expressing u_{2+} and u_{2-} in terms of u_{0+}^S and u_{0-}^S using Eqs.(16) and (17), $\sigma(R)$ takes the following simple form:

$$\sigma(R) = -2ikG\tilde{u}_0 = -kGu_0/\mathcal{D}, \quad (19)$$

$$\begin{aligned} \text{with } \mathcal{D} &= (1/2i) [(\delta_{12} - \delta_{11})e^{-ikR} - (\delta_{21} - \delta_{22})e^{ikR}] \\ &= \sin kR + \kappa_1kR \cos k(R - z_1) \cos kz_1 \\ &\quad + \kappa_2kR \cos k(R - z_2) \cos kz_2 \\ &\quad - \kappa_1\kappa_2k^2R^2 \sin k(z_2 - z_1) \cos k(R - z_2) \cos kz_1. \end{aligned}$$

The effective shear modulus $G_{\text{eff}} = -\sigma(R)R/u_0$ follows readily from Eq.(19):

$$\frac{G}{G_{\text{eff}}} = \frac{\mathcal{D}}{kR} \quad (20a)$$

$$\begin{aligned} &\simeq 1 + \kappa_1 + \kappa_2 - \frac{k^2R^2}{6} - \frac{\kappa_1 + \kappa_2}{2}k^2R^2 \\ &\quad + \kappa_1k^2z_1(R - z_1) + \kappa_2k^2z_2(R - z_2) \\ &\quad - \kappa_1\kappa_2k^2R(z_2 - z_1) + \dots \end{aligned} \quad (20b)$$

For typical numerical values, such as those used for the graphs in Fig. 1, the first two terms of the expansion of $1/G_{\text{eff}}$ with respect to kR , Eq.(20b), fall within 1% of the exact value given by Eq.(20a). The zeroth order term could have been written from scratch. The correction to the inertial mass turns out to be less transparent and is considered in the next subsection.

III.3. Effective mass

The derivation of the apparent inertia of the sample follows that given in Sec. II.2 for the homogeneous sample, starting from the same boundary conditions, Eqs.(9). Equation (10) for the integration constants is modified as:

$$\begin{aligned} \frac{u_{0+}^M}{\delta_{12}e^{-ikR} + \delta_{22}e^{ikR} - 1} &= \\ \frac{-u_{0-}^M}{\delta_{11}e^{-ikR} + \delta_{21}e^{ikR} - 1} &= \tilde{u}_0, \end{aligned} \quad (21)$$

the quantity \tilde{u}_0 being the same as in Eq.(18) for the shear modulus case.

Using these integration constants, the stress at each

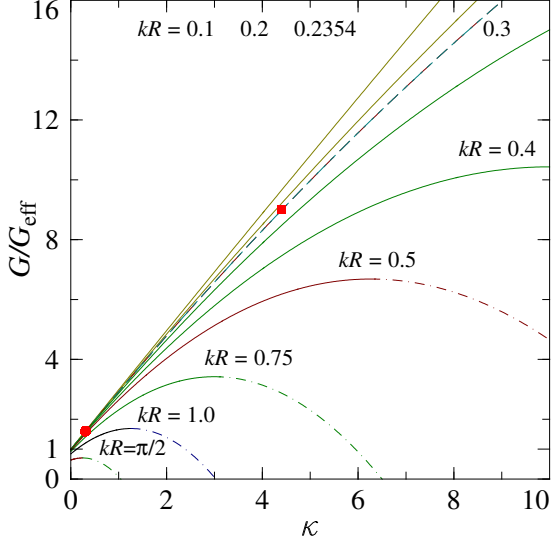


FIG. 2. Inverse effective shear modulus G_{eff} , normalised to the shear modulus with no soft layers G in terms of the dimensionless compliance κ of the soft layers, for the same parameter values as in Fig. 1 for various values of kR . The dash-dash curve represents the case with $R = 1$ cm at a frequency of one kHz, $kR = 0.2354$. The symbols mark the cases discussed in the text, (■) for $G/G_{\text{eff}} = 9$, $\kappa = 4.411$, (●) for $G/G_{\text{eff}} = 1.6$, $\kappa = 0.3075$. The dash-dot-dash lines correspond to a reentrant branch that, for a given value of G/G_{eff} , cannot be reached by adiabatic turn-on of the κ_i 's.

wall takes the following form:

$$\begin{aligned} \sigma(0) &= G \frac{du}{dz} \Big|_{z=0} = -ikG(u_{0+}^M - u_{0-}^M) \\ &= ikG\tilde{u}_0 \left[2 - (\delta_{12} + \delta_{11})e^{-ikR} - (\delta_{22} + \delta_{21})e^{ikR} \right], \\ \sigma(R) &= G \frac{du}{dz} \Big|_{z=R} = -ikG(u_{2+}e^{-ikR} - u_{2-}e^{ikR}) \\ &= -ikG\tilde{u}_0 \left[2(\delta_{11}\delta_{22} - \delta_{12}\delta_{21}) \right. \\ &\quad \left. - (\delta_{11} - \delta_{12})e^{-ikR} - (\delta_{22} - \delta_{21})e^{ikR} \right]. \end{aligned} \quad (22)$$

The total force per unit area exerted by the helium sample on both walls is now given, instead of Eq.(12) for the homogeneous case, by

$$F_X + F_R = \sigma(0) - \sigma(R) = 2ikG\tilde{u}_0 \left[2 - \delta_{11}e^{-ikR} - \delta_{22}e^{ikR} \right],$$

using again the property that $|\delta_{ij}|$ has determinant unity. Expliciting the quantities within square brackets making use of Eqs.(16) and Eq.(20a), the total force on the walls takes the final form

$$F_T = F_X + F_R = kGu_0 \frac{\mathcal{N}}{\mathcal{D}} = \frac{u_0}{R} G_{\text{eff}} \mathcal{N}, \quad (24)$$

$$\begin{aligned} \text{with } \mathcal{N} &= 2 - \delta_{11}e^{-ikR} - \delta_{22}e^{ikR} = 2(1 - \cos kR) \\ &+ (\kappa_1 + \kappa_2)kR \sin kR - \kappa_1\kappa_2k^2R^2 \sin k(z_2 - z_1) \\ &\times \left\{ \sin k(z_2 - z_1) + \sin k(R - z_2 + z_1) \right\}. \end{aligned}$$

III.4. Stationary waveforms

The displacement $u(z)$ in the sample can easily be evaluated using, *e.g.* in the inertia measurement case, the solution to the wave equation expressed by Eqs.(21) for u_{0+}^M and u_{0-}^M , with the following result:

- for slab 0: $u(z)^{(0)} = u_0[\cos kz + (B/A) \sin kz]$;
- for slab 1: $u(z)^{(1)} = u_0[\cos kz - \kappa_1 kR/2\{\sin kz + \sin k(2z_1 - z)\} + (B/A)[\sin kz + \kappa_1 kR/2\{\cos kz + \cos k(2z_1 - z)\}]]$;
- for slab 2: $u(z)^{(2)} = (u_0/A)[\sin k(R - z) + \sin kR + \kappa_1 kR/2 \cos k(z - z_1) \cos kz_1 + \kappa_2 kR/2 \cos k(z - z_2) \cos kz_2 - \kappa_1\kappa_2 K^2 G^2 \sin k(z_2 - z_1) \cos k(z - z_2) \cos kz_1]$.

In these expressions,

$$\begin{aligned} A &= (\delta'_{11} - \delta'_{12}) \sin kR + (\delta''_{12} - \delta''_{11}) \cos kR = \mathcal{D}, \\ B &= 1 - (\delta'_{11} + \delta'_{12}) \cos kR - (\delta''_{12} + \delta''_{11}) \sin kR. \end{aligned}$$

These waveforms can readily be evaluated numerically. As an example, the relative displacement $u(z)/u_0$ for three values of the dimensionless compliance κ of the soft layers, taken to be equal, is shown in Fig. 1 for $kR = 0.2354$, $z_1 = 0.3R$ and $z_2 = 0.9R$. The discontinuities at z_1 and z_2 caused by these soft layers increase in size with the compliance, up to the point where \mathcal{D} becomes zero and the deformation diverges.

The next step, carried out in the following Section, consists in extracting the parameters κ_i of the soft layers from the measured value of G_{eff} and in evaluating the corresponding apparent change in inertia.

IV. NUMERICAL RESULTS

As the temperature is raised from absolute zero, κ varies from its low temperature value, assumed to be negligibly small because the dislocations are immobilised by the isotopic impurities, to its high T value. The corresponding change of G/G_{eff} to lowest order in the small parameter kR in Eq.(20b) reduces to a static correction to the elastic constant. The lowest order correction to the effective mass results from a dynamical effect of a magnitude comparable to that of the plain elastic response, which should be subtracted out. This difference follows from Eqs.(12) and (24):

$$F_T - F_T|_{\kappa_1, \kappa_2=0} = \frac{\rho R \omega^2 u_0}{kR} \left\{ \frac{\mathcal{N}}{\mathcal{D}} - 2 \frac{1 - \cos kR}{\sin kR} \right\} \quad (25a)$$

$$\begin{aligned} &\simeq \rho R \omega^2 u_0 \frac{k^2 R^2}{1 + \kappa_1 + \kappa_2} \times \left[\frac{\kappa_1 + \kappa_2}{4} \right. \\ &\quad \left. - \kappa_1 \frac{z_1(R - z_1)}{R^2} - \kappa_2 \frac{z_2(R - z_2)}{R^2} \right]. \end{aligned} \quad (25b)$$

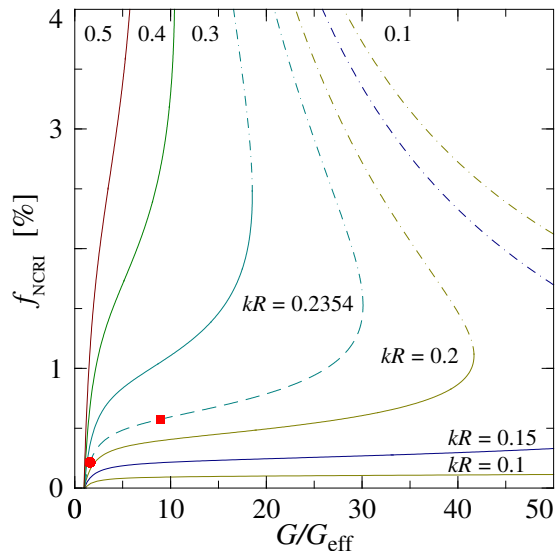


FIG. 3. Relative change in the apparent inertia, f_{NCRI} vs the inverse dimensionless shear modulus G/G_{eff} , for the situation of Fig. (1), for various values of kR as labelled in the figure. The symbols (●) and (■) on the dash-dot curve for $kR = 0.2354$ mark the same cases as in Fig. 2. The dash-dot-dash portions of the various curves correspond to reentrant regions that are not be reached by adiabatic turn-on of the compliance of the soft layers.

Equations (25a) and (25b) show how what could be called the “superfluid fraction”, $f_{\text{NCRI}} = (F_{\text{T}} - F_{\text{T}}|_{\kappa_1, \kappa_2=0})/\rho R\omega^2 u_0$ depends on the compliances κ_i , which in turn are related to the effective shear modulus. The quantity $\rho R\omega^2 u_0$ has already appeared in Eq.(12) and stands for the force due to the acceleration of the inertial mass $M_{\text{I}} = \rho R$. These quantities hold per unit area.

The full expression of the exact result, Eq.(25a), is fairly lengthy and not particularly transparent but evaluates numerically quite readily. The outcome is discussed below. The lowest order correction to this effective mass, Eq.(25b), is second order in kR and linear in the κ_i ’s, the term in $\kappa_1\kappa_2$, of order $(kR)^3$, being discarded. This correction is either positive or equal to zero for the special case $z_1 = z_2 = R/2$, that is, for a vanishing dangling mass, and, by symmetry, vanishing local stress in slab 2.

Equations (25a) and (25b), together with (20a) and (20b), which express the NCRI fraction and the effective shear modulus in the presence of soft dislocation arrays, constitute the main result of this work.^{34,54}

The variation of the shear modulus in terms of the soft layer compliances, taken for simplicity to be equal to a common value κ , is shown in Fig. 2 for various values of kR for the same sample geometry and parameter values as in Fig. 1. As the compliance κ increases from zero, assumed to be its $T = 0$ value, the effective shear modulus G_{eff} decreases; the solid becomes softer, up to a point

where G/G_{eff} reaches a maximum: the interfaces between slab 1 and its neighbours becomes so soft that, although the dangling slab swings with increasing amplitude, the stress due to its motion ceases to increase. Beyond this point, a further increase in κ would lower G/G_{eff} because the stress reflected back onto the external boundaries effectively decreases while the displacement of slab 1 goes on increasing.

It has been assumed above that the steady-state regime is reached adiabatically, which implies: 1) that only the ascending branch of G/G_{eff} in Fig. 2 can be reached by adiabatic turn-on of the κ_i ’s from zero; 2) that damping does not vanish entirely. If damping is introduced in the wave equation, Eq.(2), slab 1 would be coupled to its neighbours by friction in addition to shear elasticity and the results obtained above would be quantitatively different from those in Fig. 2 for very small values of G_{eff} . In particular, the descending branch of $G/G_{\text{eff}}(\kappa)$ could not actually cross the x -axis.

The NCRI fraction is plotted directly in terms of the shear modulus in Fig. 3. From the measured overall change in G/G_{eff} , which reaches values of 1.6^{22,28} up to 9 or more,²⁹ the corresponding values of the compliance of the soft layers can be found from Eq.(20a). From these values, $\kappa = 0.31$ for $G/G_{\text{eff}} = 1.6$, $\kappa = 4.4$ for $G/G_{\text{eff}} = 9$, the NCRI fractions given by Eq.(25a) are 0.22 % and 0.58 % respectively. These values depend on z_1 and z_2 : the largest f_{NCRI} are achieved for $z_1 \sim 0$, $z_2 \sim R$. The reentrant branches of the graphs in Fig. 3 correspond to the descending branches for large κ in Fig. 2. An accurate description of these regimes where displacements become very large should, as already mentioned, include damping. They are irrelevant to the present discussion.

Dislocations are also found in the homogeneous slabs. They may also induce a variation of $k = \sqrt{\rho/G}\omega$ as G may also vary with temperature. The contributions to f_{NCRI} of the soft layers and of the dislocation network in the homogeneous slabs are seen in Eq.(25a) to be additive and their respective weights depend on how each contributes to G/G_{eff} . However, the contribution of the network should be no more than 20%, the geometrical limit for hcp structures, so that its effect on f_{NCRI} is less significant.

The highest values of f_{NCRI} for given G/G_{eff} and kR are reached for $z_1 = 0$, $z_2 = R$ and varying κ_1 while adjusting κ_2 to keep G/G_{eff} constant. These *maximum maximum* values are plotted in Fig. 4 for $kR = 0.2354$ and 0.1, and for various values of the effective shear modulus. These quantities overtake those for homogeneous systems, given by Eqs.(8) and (12), up to G/G_{eff} values that are much larger than those for homogeneous systems $\Lambda L_{\text{N}}^2 \leq 2^{-1/2}$, as seen in Fig. 4. Values of f_{NCRI} ranging from near zero to above one per cent can be reached for $kR = 0.2354$, *i.e.* in a one cm size cell at a frequency of 1 kHz for the experimentally observed values of G/G_{eff} . For a cylindrical geometry, these values are approximately halved.⁵⁵

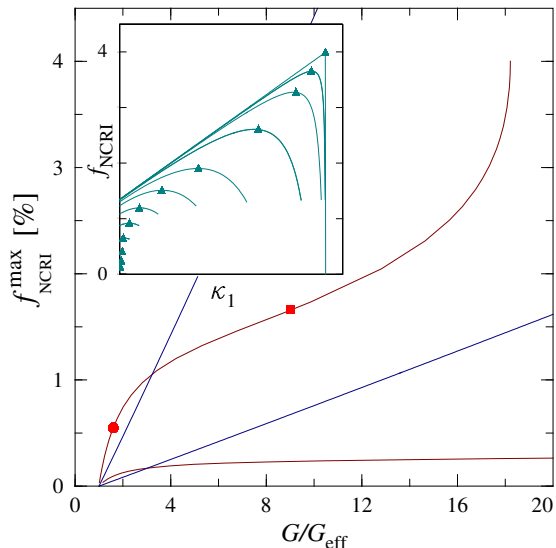


FIG. 4. Maximum possible value of f_{NCRI} in terms of G/G_{eff} for $kR=0.2354$ (upper curves) and 0.1 (lower curves). The nearly straight curves stem from the homogeneous elastic response, the bending curves are the pure soft layer contributions. The values for $f_{\text{NCRI}}^{\text{max}}$ are extracted from graphs for f_{NCRI} in terms of κ_1 as shown in the insert where they are marked by (\blacktriangle) . The symbols (\bullet) and (\blacksquare) on the curve for $kR = 0.2354$ mark the same cases as in Fig. 2.

V. DISCUSSION

Because of the very large drop of the shear modulus observed at low frequencies in most samples of solid ^4He , it is surmised in this work that, instead of forming homogeneous random networks, dislocations crop into organised slip bands or quasi-planar arrays of sizable thickness. When the ^3He impurities evaporate from the cores of the dislocation lines, the latter become very mobile and the planar arrays very soft.⁴⁸ It is argued that a large degree of polycrystallinity does not suffice to obtain large G/G_{eff} and large f_{NCRI} , as shown experimentally in aerogel by Mulders *et al.*⁵⁶ Dislocations have to organise over large distances in such a way that parts of the sample become uncoupled and acquire additional kinetic energy, thereby increasing the apparent inertia.

In a hcp structure, edge dislocations glide easily in the basal plane along three preferred crystallographic directions at 120 degrees of one another. To climb away from these directions, they have to change into screw or mixed dislocations. As shown by Suzuki and Nishioka⁵⁷ this process is thermally assisted above ~ 0.8 K (at $\rho = 0.192$ g/cm³) and proceeds by quantum-tunnelling below. More recent and detailed theoretical considerations of the climb process in the quantum regime^{58,59} have led to the realisation that the cores of screw and edge dislocations could become superfluid. Climb processes would then become greatly enhanced, hence the concept of “super-climb” introduced by Kuklov and coworkers.^{60–63} This

quantum-assisted climb process provides a mechanism in solid ^4He for edge dislocations to easily move off the basal plane. This process lifts a constraint on dislocation motion. The propagation of dislocation pile-ups in the course of plastic deformation becomes greatly facilitated, as well as the formation of percolating planar defects.

On heuristic grounds, propagation of dislocation pile-ups in brittle materials, such as hcp helium, causes cracks to form and results eventually in mechanical failure. In solid helium, which is under positive hydrostatic pressure, cracks with voids cannot form but corresponding macroscopic defects with little or no crystalline order must appear.^{48,50} Hence the plausible appearance of connected veins imprinted by plastic flow. These regions of the sample show strong spatial disorder and can possibly sustain off-diagonal long range order instead.^{1,64} That they are found anomalously soft in a number of experiments lends credence to this possibility.

The model based on these soft layers is easily tractable analytically. The calculated values for the shear modulus and the NCRI fall within the range of observed values, barring the highest ones.⁶⁵ This model explains readily why the NCRI and stress-strain measurements depend so strongly on the sample geometry⁶⁵ and thermal history:^{55,66} even small changes in the soft layer properties and the interconnection of the channels that they delimit can greatly influence the motion of the dangling masses. Homogeneous dislocation networks, besides having a limited effect of the shear modulus, can hardly exhibit such variability.

Actual samples studied in the laboratory are likely to be more convoluted than sketched in Fig. 1. The veins have tortuous paths and coarse sheaths, which might appear to hinder motion. However, applied strains are small, of the order of 10^{-6} or less,^{28,46,67} and displacements are correspondingly small. The soft layers considered here are thicker than low-tilt angle subgrain boundaries, possibly in the 10 to 100 nm range.⁴⁸ The crystal lattice is heavily distorted over such a thickness. The soft layers can be expected to be quite malleable on such a scale and yield easily under local stress. Being extremely compliant, they support plastic flow within themselves and accommodate departures from the ideal planar geometry depicted in Fig. 1. The soft layers can conceivably also become fully fluid,³⁸ or even genuinely superfluid as already mentioned above.⁶⁴ Crystal subgrain motions on a sub-millimetric scale have actually been reported by Burns *et al.*¹⁹ in X-ray experiments using very fine collimated beams. Similarly, the mobile features observed in solid ^4He at higher temperatures^{68–70} can be re-examined in the present framework; these experiments also provide possible clues for the existence of veins of easy deformation.

Maris and Balibar⁷¹ take a quite different point of view to account for the observed relationship between G_{eff} and f_{NCRI} . They point out that experimental TO’s may lack sufficient structural rigidity. If the TO body deforms in such a way as to induce additional strain on the helium

sample, the NCRIf may appear larger than the intrinsic value. As discussed in Ref.[71], the effect can be quite large. This helps in particular to understand some very large NCRIf values reported in the literature^{8,32} that would not be readily explainable with the existence of soft layers as assumed here. From the results in Figs.3 and 4, f_{NCRIf} remains below a few percent at the most for centimetre size cells, less for smaller toroidal annuli. But conversely, these results do not imply that, whenever the stiffness of the helium sample changes, an apparent NCRIf is bound to occur; this last feature depends on the geometry of the soft layers and may be altogether absent.⁷²

A number of experiments might seem to invalidate the present approach. The TO experiments with a blocked channel show a much reduced NCRIf. This is interpreted as the manifestation that some sort of superflow is taking place when flow paths are connected in a loop and not when the loop is broken. However, the same considerations apply to the plastic flow in connected veins, which also can form, or not, channels through which dangling masses can jiggle.

Torsional oscillator measurements in confined geometries, Vycor, porous gold, aerogel, . . . , do show a sizable NCRIf and would also appear to completely invalidate the present approach. If the model is applied to a single pore, for which kR is very small, then, indeed, the resulting effect that decreases as $(kR)^2$ will be extremely small. For sizes comparable to that of the soft layers, the soft layer model is not expected to apply, neither for shear nor for inertia. Pores do not appear to be filled with homogeneous hcp solid but with either a combination of layers of liquid and of bcc solid¹⁶ on top of 1~2 layers of amorphous solid, or, for finer pores (47 Å in MCM-41 and 34 Å in gelsil),¹⁷ with amorphous solid only and inclusions of bcc-like nodules. What was assumed for softer layers carries over to the fine pores, which present a multi-connected geometry with complex plastic flow patterns. The conditions of existence of connected veins assumed at a macroscopic level are clearly fulfilled at the mesoscopic level of the pores so that helium, either liquid or amorphous, would contribute to NCRIf. These questions deserve further consideration.^{33,71}

Hexagonal solid ³He is also soft but appears not to show NCRIf: the two isotopes apparently possess similar elastic properties but different inertial properties. This isotopic dependence is well documented, in particular by the work of West *et al.*⁹. This observation would seem to also invalidate the present approach. However, the tunnelling motion of dislocations is unlikely to proceed in a similar manner in the bosonic and fermionic solids. In particular, the process of superclimb,⁶⁰⁻⁶³ which may assist the formation of connected plastic flow veins, relies on the existence of superfluidity in dislocation cores.^{58,59} This mechanism does not operate in solid ³He.

Kim *et al.*³¹ directly addressed the connexion between shear and NCRIf in an ingenious experimental arrangement allowing simultaneous measurements of both quan-

ties. They observe, in particular, that the response to an increase in drive amplitude differs very significantly between both properties. However, the drive is not applied in an identical manner for both measurements because of details of the cell geometry. Soft layers can be located at different places and have different conformations: they are bound to respond differently.

Specific experiments can be performed to probe the present model. Shear modulus measurements have not been performed in a cell geometry for which the plastic flow lines would close on themselves in the way they do in torsional oscillators. These measurements should reveal the existence of supersoft elastic moduli.⁷⁰ Equipping a torsional oscillator with a floppy membrane as *septum* to interrupt a quantum-coherent flow but not the continuity of stresses and strains offers another venue.⁷³ The study of higher resonance modes in multiply-connected acoustic cavities can also provide a way to probe the internal response of an inhomogeneous sample.⁷⁴

Multiple-mode TO resonators^{32,75,76} appear to give somewhat indecisive answers but still show the expected trend of enhanced NCRIf at higher frequency.³³ A two-mode TO with the dummy massive bob *inside* the resonator chamber, in contact with the solid helium but connected loosely to the main body by an additional torsion rod provides a mean of coupling shear to the sample in a Couette-type experiment. If the inner bob angular position could be tracked by some optical or electro-dynamical means, the coupled system response could be analysed in detail. A strong enhancement of G/G_{eff} is expected, which would be directly related to the NCRIf. A control experiment with bcc ³He, which shows no shear modulus anomaly and no NCRIf,⁹ can be carried out at appropriate density and shear modulus values to distinguish between cell and sample contributions to the apparent NCRIf.

To conclude, the soft layer model presented here takes into account known heterogeneities in dislocation patterns revealed in particular by the anomalous softening of most samples of hcp ⁴He. It is argued that the actual softness can be even more extreme than observed, being hampered by the tortuous arrangement of the dislocation structures and of the crystalline regions that they delimit. The corresponding values of the NCRIf are shown to lie within the range of observations, barring the highest ones. The model conflicts in no irredeemable way with the available assortment of experimental observations. Conversely, it can be stated that most existing experiments to date support the assumption of the existence of very mobile macroscopic veins arranged along connected paths in hcp crystals of helium 4 and formed in a process that depends on quantum statistics, like superclimb. Matter in the veins themselves undergoes displacements governed by classical mechanics and subject to dissipative mechanisms. These various assertions are amenable to experimental verification.

ACKNOWLEDGMENTS

The author acknowledges useful discussions with Izumi Iwasa, Sébastien Balibar and Yuri Mukharsky and correspondence with John Reppy. He thanks Alan Braslau for his numerous suggestions on the manuscript. This work has been supported by ANR grant “Superdur”.

* eric.varoquaux@cea.fr

- ¹ O. Penrose and L. Onsager, Phys. Rev., **104**, 576 (1956).
- ² A. Andreev and I. Lifshits, Sov. Phys. JETP, **29**, 1107 (1970).
- ³ G. Chester, Phys. Rev. A, **2**, 256 (1970).
- ⁴ A. Leggett, Phys. Rev. Lett., **25**, 1543 (1970).
- ⁵ N. Prokof'ev, Advances in Physics, **56**, 381 (2007); S. Balibar and F. Caupin, J. Phys. Cond. Mat. **20**, 173201 (2008); D.E. Galli and L. Reatto, J. Phys. Soc. Jpn., **77**, 585 (2008).
- ⁶ L. Landau and E. Lifshitz, “Fluid mechanics,” (Pergamon Press, London, 1959) Chap. XVI, p. 510.
- ⁷ E. Kim and M. Chan, Science, **305**, 1941 (2004).
- ⁸ A. S. C. Rittner and J. D. Reppy, J. Low Temp. Phys., **101**, 155301 (2008).
- ⁹ J. T. West, O. Syshchenko, J. Beamish, and M. H. W. Chan, Nature Physics, **5**, 598 (2009), see also the review by J. Beamish, to appear in the J. Low Temp. Phys.
- ¹⁰ S. Sasaki, F. Caupin, and S. Balibar, Phys. Rev. Lett., **99**, 205302 (2007).
- ¹¹ J. Day and J. Beamish, J. Low Temp. Phys., **148**, 627 (2007).
- ¹² A. S. C. Rittner, W. Choi, E. J. Mueller, and J. D. Reppy, Phys. Rev. B, **80**, 224516 (2009).
- ¹³ M. W. Ray and R. B. Hallock, Phys. Rev. B, **79**, 224302 (2009).
- ¹⁴ S. Kwon, N. Mulders, and E. Kim, J. Low Temp. Phys., **158**, 590 (2010).
- ¹⁵ Y. Aoki, H. Kojima, and X. Lin, Low Temp. Phys., **34**, 329 (2008).
- ¹⁶ D. Wallacher, M. Rheinstaedter, T. Hansen, and K. Knorr, J. Low Temp. Phys., **138**, 1013 (2005).
- ¹⁷ J. Bossy, T. Hansen, and H. R. Glyde, Phys. Rev. B, **81**, 184507 (2010).
- ¹⁸ S. Diallo, R. Azuah, and H. Glyde, J. Low Temp. Phys., **162**, 449 (2011).
- ¹⁹ C. A. Burns, N. Mulders, L. Lurio, M. H. W. Chan, A. Said, C. Kodituwakku, and P. M. Platzman, Phys. Rev. B, **78**, 224305 (2008).
- ²⁰ R. Wanner, I. Iwasa, and S. Wales, Solid State Com., **18**, 853 (1976).
- ²¹ V. Tsymbalenko, Sov. Phys. JETP, **47**, 787 (1978).
- ²² V. Tsymbalenko, Sov. Phys. JLTP, **49**, 859 (1979).
- ²³ I. Iwasa, K. Araki, and H. Suzuki, J. Phys. Soc. Japan, **46**, 1119 (1979).
- ²⁴ I. Iwasa and H. Suzuki, J. Phys. Soc. Jpn., **49**, 1722 (1980).
- ²⁵ M.A. Paalanen, D.J. Bishop, and H.W. Dail, Phys. Rev. Lett., **46**, 664 (1981).
- ²⁶ J. Day and J. Beamish, Nature (London), **450**, 853 (2007).
- ²⁷ J. Day and J. Beamish, J. Low Temp. Phys., **148**, 683 (2007).
- ²⁸ Y. Mukharsky, A. Penzev, and E. Varoquaux, Phys. Rev. B, **80**, 140504 R (2009).
- ²⁹ X. Rojas, A. Haziot, V. Bapst, S. Balibar, and H. J. Maris, Phys. Rev. Lett., **105**, 145302 (2010).
- ³⁰ J. Reppy, Phys. Rev. Lett., **104**, 255301 (2010).
- ³¹ D. Y. Kim, H. Choi, W. Choi, S. Kwon, E. Kim, and H. C. Kim, Phys. Rev. B, **83**, 052503 (2011).
- ³² X. Mi, E. Mueller, and J. D. Reppy, arXiv:1109.6818.
- ³³ J.D. Reppy, private communication.
- ³⁴ A preliminary version of this work has been posted on arXiv:1107.2296.
- ³⁵ Z. Nussinov, A. V. Balatsky, M. J. Graf, and S. A. Trugman, Phys. Rev. B, **76**, 014530 (2007).
- ³⁶ C.-D. Yoo and A. T. Dorsey, Phys. Rev. B, **79**, 100504 (2009).
- ³⁷ I. Iwasa, Phys. Rev. B, **81**, 104527 (2010).
- ³⁸ H. Suzuki, J. Phys. Soc. Japan, **35**, 1472 (1973).
- ³⁹ H. Suzuki, J. Phys. Soc. Japan, **42**, 1865 (1977).
- ⁴⁰ D. Sanders, H. Kwun, A. Hikata, and C. Elbaum, Phys. Rev. Lett., **39**, 815 (1977).
- ⁴¹ Y. Hiki and F. Tsuruoka, Phys. Lett., **62A**, 50 (1977).
- ⁴² F. Tsuruoka and Y. Hiki, Phys. Rev. B, **20**, 2702 (1979).
- ⁴³ O. Syshchenko, J. Day, and J. Beamish, Phys. Rev. Lett., **104**, 195301 (2010).
- ⁴⁴ A. Granato and K. Lücke, Appl. J. Phys., **27**, 583 (1956).
- ⁴⁵ J. Day, O. Syshchenko, and J. Beamish, Phys. Rev. B, **79**, 214524 (2009).
- ⁴⁶ J. Day, O. Syshchenko, and J. Beamish, Phys. Rev. Lett., **104**, 075302 (2010).
- ⁴⁷ J. Friedel, *Dislocations*, first edition with corrections ed. (Pergamon Press, 1967) §8.5.2.
- ⁴⁸ R. Amodeo and N. Ghoniem, Phys. Rev. B, **41**, 6968 (1990).
- ⁴⁹ H. M. Zbib, M. Rhee, and J. P. Hirth, Int. J. Mech. Sci., **40**, 113 (1998).
- ⁵⁰ S. Takeuchi and A. Argon, J. Mat. Sc., **11**, 1542 (1976).
- ⁵¹ I. Iwasa, H. Suzuki, T. Suzuki, T. Nakajima, I. Yonenaga, H. Suzuki, H. Koizumi, Y. Nishio, and J. Ota, J. Low Temp. Phys., **100**, 147 (1995).
- ⁵² J. Bossy, P. Bastie, P. Averbuch, O. Losserand, P. Courtois, Y. Mukharsky, and A. Braslau, J. Low Temp. Phys. (to be published).
- ⁵³ J. Hirth and J. Lothe, *Theory of Dislocations* (McGraw-Hill, 1968) ch. 21.
- ⁵⁴ The relation between f_{NCRI} and G_{eff} reported in Ref.[37] should stem from the present Eqs.(8) and (12) for the homogeneous sample with G replaced by G_{eff} . This corrected result is obtained directly by applying the boundary condition at the wall of the torsional oscillator to the full displacement $u(r, t)$ instead of just to the elastic part $u_{el}(r, t)$ in Eq.(22) of Ref.[37]. The same modification holds in Eq.(23) and leads to the cancellation of first order correction in kr to the TO period. The second order term is

that obtained by A.C. Clark, J.D. Maynard, and M.H.W. Chan⁵⁵ for a cylindrical geometry.

- ⁵⁵ A.C. Clark, J.D. Maynard, and M.H.W. Chan, Phys. Rev. B, **77**, 184513 (2008), result (13) differs by a numerical factor from that of this reference, but pertains to a planar geometry instead of a cylindrical one.
- ⁵⁶ N. Mulders, J. West, M. Chan, C. Kodituwakku, C. Burns, and L. Lurio, Phys. Rev. Lett., **101**, 165303 (2008).
- ⁵⁷ H. Suzuki and Y. Nishioka, “Dislocation in solids,” (University of Tokyo Press, 1985) p. 169.
- ⁵⁸ S. Shevchenko, Sov. J. Low Temp. Phys., **13**, 61 (1987).
- ⁵⁹ M. Boninsegni, A. B. Kuklov, L. Pollet, N. V. Prokof'ev, B. V. Svistunov, and M. Troyer, Phys. Rev. Lett., **99**, 035301 (2007).
- ⁶⁰ D. Aleinikava, E. Dedits, A. Kuklov, and D. Schmeltzer, “Mechanical and superfluid properties of dislocations in solid ^4He ,” (2008), arXiv:0812.0983.
- ⁶¹ S.G. Söyler, A.B. Kuklov, L. Pollet, N.V. Prokof'ev, and B.V. Svistunov, Phys. Rev. Lett., **103**, 175301 (2009).
- ⁶² D. Aleinikava, E. Dedits, A. B. Kuklov, and D. Schmeltzer, Europhys. Lett., **89**, 46002 (2010).
- ⁶³ D. Aleinikava, E. Dedits, and A. Kuklov, J. Low Temp Phys, **162**, 464 (2011).
- ⁶⁴ M. Boninsegni, N. Prokof'ev, and B. Svistunov, Phys. Rev. Lett., **96**, 105301 (2006).
- ⁶⁵ A. S. C. Rittner and J. D. Reppy, J. Low Temp. Phys., **148**, 671 (2007).
- ⁶⁶ Y. Mukharsky, O. Avenel, and E. Varoquaux, J. Low Temp. Phys., **148**, 689 (2007).
- ⁶⁷ O. Syshchenko, J. Day, and J. Beamish, J. Phys.: Condens. Matter, **21**, 1 (2009).
- ⁶⁸ A. Eyal, O. Pelleg, L. Embon, and E. Polturak, Phys. Rev. Lett., **105**, 025301 (2010).
- ⁶⁹ A. Eyal and E. Polturak, J. Low Temp. Phys., DOI 10.1007/s10909 (2011).
- ⁷⁰ The experiments of Sanders et al. [40] and of Ray and Hallock [13], which provide “open ended” boundary conditions to helium atoms, offer the closest realisations of the thought-experimental model considered here.
- ⁷¹ H. J. Maris and S. Balibar, J. Low Temp. Phys., **160**, 5 (2010).
- ⁷² A. Fefferman, X. Rojas, A. Haziot, S. Balibar, J. West, and M. Chan, “ ^4He crystal quality and rotational response in a transparent torsional oscillator,” (2011), arXiv:1112.5998.
- ⁷³ Y. Mukharsky, private communication.
- ⁷⁴ Y. Mukharsky and A. Penzev, J. Low Temp. Phys. (2012), to be published.
- ⁷⁵ Y. Aoki, X. Lin, and H. Kojima, J. Low Temp. Phys., **148**, 659 (2007).
- ⁷⁶ Y. Aoki, J. C. Graves, and H. Kojima, J. Low Temp.

Phys., **150**, 252 (2008).

Appendix:

In a crystal lattice with hexagonal symmetry, there exists three glide directions for edge dislocations in the basal plane, perpendicular to the \hat{c} -axis, at $2\pi/3$ from one another. These dislocations arrange themselves on a hexagonal network in the basal plane with side length a , possibly connected to adjacent basal planes at a distance c along the \hat{c} -axis by pillars of screw or mixed dislocations.

The dislocation network that entirely fills a given basal plane of a sample taken as a square of side S for simplicity, can be constructed as shown in Fig. 5. The building block in thicker line is duplicated and translated by \vec{A} along one side and \vec{b} along the other. There are a total of S^2/bA such translations, each involving a dislocation line length equal to $6a$. The volume spanned in the process is S^2c so that the density of edge dislocation amounts to $\Lambda = 6a/bAc$. As $b = 3^{1/2}a$ and $A = 3a$, there comes that $\Lambda ac = 2/3^{1/2}$. This result has already been quoted by Iwasa *et al.*²³.

The network length L_N can be taken equal to a ; it disappears in the final result for ΛL_N^2 , which is scale-independent. For a hexagonal close packed lattice, $c = (8/3)^{1/2}a$ so that the expression ΛL_N^2 in Eq.(1) takes the value $2^{-1/2}$. This value is smaller if the lattice is less densely packed. For a cubic lattice, a similar derivation gives the often quoted geometrical limit $\Lambda L_N^2 = 3$, a value much larger than for a hexagonal lattice. This result reflects the paucity of easy glide directions in the latter case.

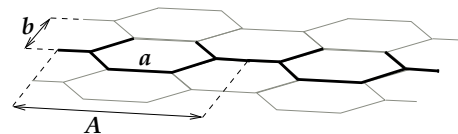


FIG. 5. Dislocation network in a hexagonal structure. The network is formed of 2D hexagonal cells, of side length a in basal planes perpendicular to the \hat{c} -axis. The whole pattern can be generated from the elementary block in thick line of length A by translations of moduli A and b as shown in the figure.